ACS OMEGA

Article

Cite This: ACS Omega 2018, 3, 1509−1521

Design of a Multifunctional Nanoengineered PLLA Surface by Maximizing the Synergies between Biochemical and Surface Design Bactericidal Effects

Maria Nerantzaki,[†] Nikolaos Kehagias,[‡] Achille Francone,[‡] Ariadna Fernández,[‡] Clivia M. Sotomayor Torres,[‡,§] Rigini Papi,[†] Theodora Choli-Papadopoulou,[†] and Dimitrios N. Bikiaris*[,†]

[†]Department of Chemistry, Aristotle University of Thessaloniki, GR-541 24 Thessaloniki, Macedonia, Greece

[‡]Catalan Institute of Nanoscience and Nanotechnology (ICN2), CSIC and BIST, Campus UAB, Bellaterra, 08193 Barcelona, Spain

[§]ICREA, Institució Catalana de Recerca i Estudis Avançats, Pg. Lluís Companys 23, 08010 Barcelona, Spain

ABSTRACT: Nanotechnology, the manipulation of matter on atomic, molecular, and supramolecular scales, has become the most appealing strategy for biomedical applications and is of great interest as an approach to preventing microbial risks. In this study, we utilize the antimicrobial performance and the drug-loading ability of novel nanoparticles based on silicon oxide and strontium-substituted hydroxyapatite to develop nanocomposite antimicrobial films based on a poly(L-lactic acid) (PLLA) polymer. We also demonstrate that nanoimprint lithography (NIL), a process adaptable to industrial application, is a feasible fabrication technique to modify the surface of PLLA, to alter its physical properties, and to utilize it for antibacterial applications. Various nanocomposite PLLA films with nanosized (black silicon) and three-dimensional (hierarchical) hybrid domains were fabricated by thermal NIL, and their bactericidal activity against *Escherichia coli* and *Staphylococcus aureus* was assessed. Our findings demonstrate that besides hydrophobicity the nanoparticle antibiotic delivery and the surface roughness are essential factors that affect the biofilm formation.

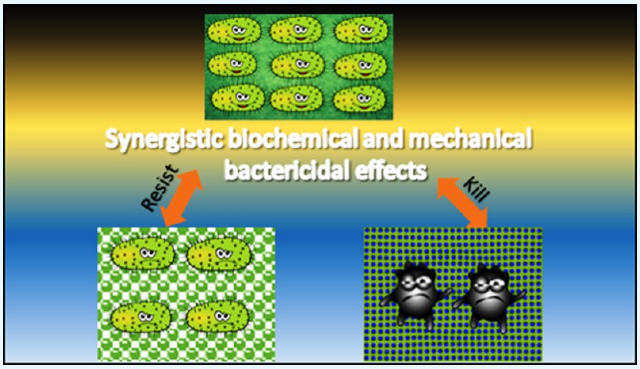

1. INTRODUCTION

The tendency of bacterial cells to adhere to and colonize a material surface is a fundamental challenge underlying various biomaterial-associated applications ranging from surgical sutures to tissue engineering scaffolds, medical implants, and drug-eluting devices.[1,2] To eliminate or substantially reduce the extent of bacterial attachment and biofilm formation on biomaterial surfaces, intensive efforts have been focussed on the development of new surfaces or on the improvement of the performance of existing antibacterial materials.[3]

New strategies for designing antibacterial substrates, mediated by topographical features of micro- and/or nanometer scales, are gaining increasing interest aside from the conventional chemistry-based approaches.[4] On such a geometrically patterned surface, the bacteria are enclosed and are surrounded by slopes, slants, walls, wells, or other architectural shapes. In a recent report, nanoscale-inspired microdomains on a polyurethane catheter were shown to reduce bacterial colonization of the surface.[5] The confined surface topography with pillars of defined geometric shapes limits the attachment such that bacteria have less contact area between the pillars on the surface when compared to that on smooth unpatterned substrates. In fact, biomimicry of antibacterial surfaces in nature is a popular strategy. These kinds of antibacterial surface-treated substrates were first explored on shark skin and lotus leaves, and a due acknowledgment must be given to these early findings.[6]

The nanocomposite approach has been also proved to be significantly beneficial for the preparation of bactericidal surfaces. Nanostructured noble metals with considerable antimicrobial activity, most commonly, silver in its various forms (nanoparticles, nanolayers, and nanowires, etc.), might be used effectively.[7,8] These antimicrobial agents (i) might be incorporated throughout the volume of polymeric matrix or (ii) might form coatings on the polymeric surface. Their presence in the polymer matrix causes the reduction of initial microbial adhesion to surfaces and inactivation of microorganisms already adherent to a surface. An additional advantage of nanoparticles is their high surface-area-to-volume ratio. This property, in comparison with the high porosity of nanoparticles in some cases, enables high loading of therapeutics like drugs, with

Received: November 9, 2017
Accepted: January 16, 2018
Published: February 5, 2018

DOI: 10.1021/acsomega.7b01756
ACS Omega 2018, 3, 1509−1521

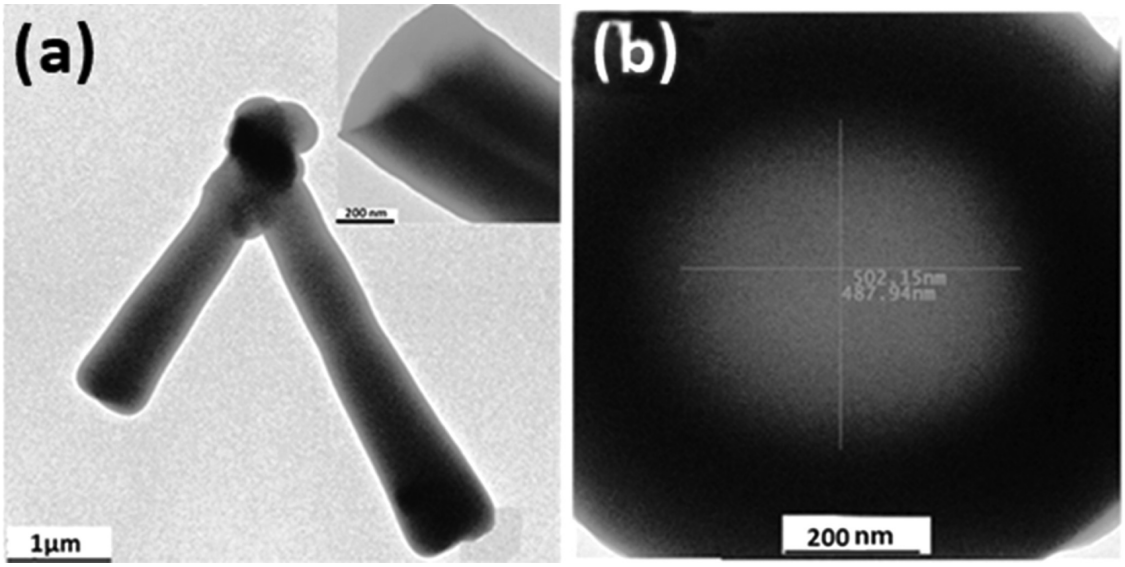

Figure 1. TEM observations of SiO_2 ntbs at a (a) low and (b) high resolution.

promising synergy arising from multivalent interactions between drugs and the surface of nanoparticles.[9,10]

Given this foundation, in this study, nanoparticle-based antibiotic carriers like mesoporous strontium hydroxyapatite nanorods (SrHA nrds) and silica nanotubes (SiO_2 ntbs) will be prepared and used for chloramphenicol (CAM) antibiotic drug loading and re-engineered to not only attack and kill but also nonlethally manipulate the physiologies of bacteria. In particular, sol−gel-synthesized SrHA nrds, because of their inner space that can be filled by pharmaceutical molecules and because of the antibacterial properties of strontium ions, have been investigated as antibiotic carriers with bactericidal effect.[11,12] In addition, tailored SiO_2 ntbs with tunable surface functionality and multivalency have been synthesized using a facile sol−gel route and examined for their potential to entrap antibiotics and target bacteria.[13] These nanoparticles will be used for the preparation of antibacterial film nanocomposites with poly(lactic acid) containing 1 wt % SrHA nrds or SiO_2 ntbs loaded with chloramphenicol (CAM) drug.

Except nanoparticles or drugs, it was reported that polymer surfaces also play an important role in antibacterial activity.[14] For example, it was found that "black silicon" (BS) and nanopillar-type structures are the most effective surfaces with appropriate bactericidal properties. The bactericidal action through physical surface topography, which has been associated with the deforming stress applied by these nanoarchitectures, is highly dependent on certain external factors, including the size, shape, density, rigidity/flexibility, and surface chemistry of the surface nanotextures, as well as factors such as bacterial specificity (e.g., Gram-positive and Gram-negative) and motility.[6] Thus, in the present study, to maximize the antibacterial properties of CAM-loaded nanoparticles, similar nanostructures of poly(L-lactic acid) (PLLA) nanocomposites in the form of thin films will be prepared using nanoimprint lithography (NIL). By integrating the most remarkable strategies for designing antibacterial coatings, nanocomposite approach, and the implementation of micro- and nanosized topographies, we aim at fabricating antimicrobial-treated films based on PLLA. Owing to its beneficial properties, such as high mechanical strength, excellent thermoforming ability, biocompatibility, and monomer renewability, PLLA is the most widely used polyester for biomedical applications.[15,16]

2. RESULTS AND DISCUSSION

2.1. Physicochemical and Morphological Study of SrHA nrds and SiO_2 ntbs. Sol−gel techniques have been extensively used to form silica gel nanotubes and mesoporous silica nanotubes.[17−19] Adachi et al. were the first to study surfactant-assisted growth for the formation of very long silica nanotubes.[20] Here, tube formation was followed by trimethylsilylation treatment, using citric acid (CA) as a structure modifier. The main advantage of the trisylation treatment is that it inactivated the silanol groups among the different bundles, yielding long individual SiO_2 ntbs, whereas another advantage of the method used is that the surfactant was removed without calcination. Moreover, previous reported results confirm that both the use of CA and external synthetic conditions control the formation of particular structures of silica. In contrast, a rapid addition of ammonia and CA under static conditions leads to the formation of micrometer-sized rods with uniform morphologies.[17] Here, the slow addition of ammonia/CA under vigorous stirring was ideal for the development of desired silica structures.

Figure 1a gives the transmission electron microscopy (TEM) image of the as-synthesized SiO_2 ntbs. It is shown that long single-wall nanotubes with uniform wide diameters together with some nanoparticles coexisted in the as-synthesized powder. The length of the tubes ranged from hundreds of nanometers to tens of micrometers (~0.5−20 μm). From the high-magnification image of a typical nanotube (Figure 1b), it can be seen that the center of the material is light and both the edges are dark, showing the well-defined structure of the nanotube. The inner diameters of the tubes are about 500 and 130 nm and the outer diameters of nanotubes vary from 800 to 100 nm, whereas the head part of the tube indicates that the channel is open (Figure 1b). SiO_2 ntbs are the novel nanoparticles that exhibited excellent possibilities as multifunctional drug carriers. More particularly, nanotubes with open ends, which allow both inside and outside surfaces to interact with drug molecules, offer a large surface-to-volume ratio and thus improve the drug-loading capacity.[21]

DOI: 10.1021/acsomega.7b01756
ACS Omega 2018, 3, 1509−1521

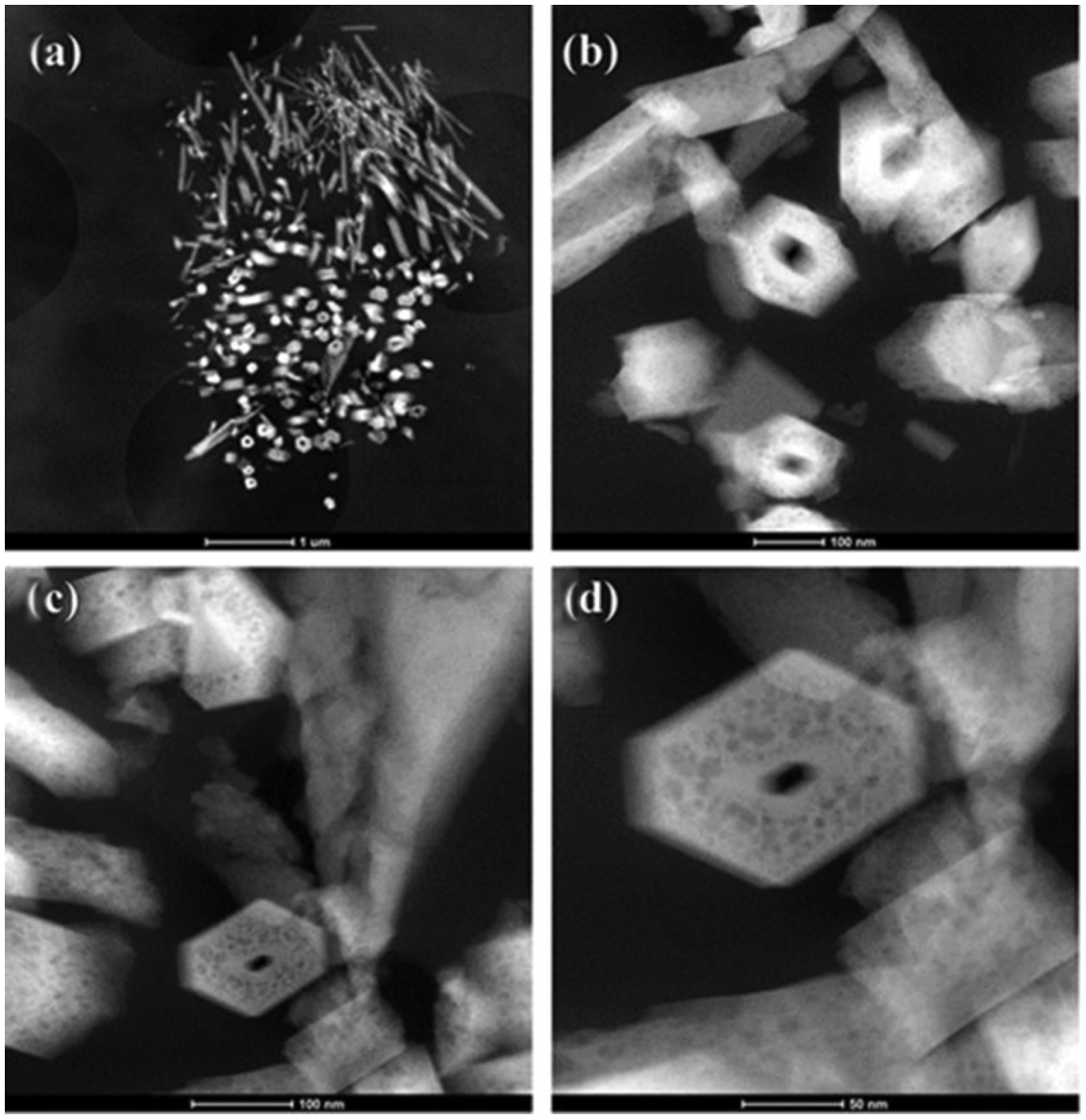

Figure 2. (a−d) Low- and high-angle annular dark-field scanning transmission electron microscopy images of SrHA nrds where the mesopores are observed.

It is well proven that different methods, such as co-precipitation, sol−gel technique, solid-state reaction, combustion technique, spray pyrolysis, hydrothermal method, microwave irradiation process, etc., can be employed for the synthesis of nanohydroxyapatite with controlled structural and morphological characteristics.[22,23] Here, as demonstrated through TEM observations in Figure 2, SrHA nrds were successfully synthesized via a simple hydrothermal synthesis (sol−gel) route, with average length of 200−400 nm and diameter of ∼20 nm. In Figure 2c,d, it is well documented that mesoporous structures were successfully introduced into the as-obtained SrHA nanorods because of the presence of organic additive cetyltrimethyl-ammonium bromide (CTAB) during the hydrothermal synthesis, followed by the treatment with refluxing acetone to remove it. Mesoporosity is very important because it not only offers high surface area that could be used to conjugate different functional groups but also provides a large accessible pore volume for small absorbable biomolecules or even functional nanoparticles.[24]

The chemical compositions of SiO_2 ntbs and SrHA nrds were studied by Fourier transform infrared (FT-IR) spectroscopy. The broad peak from 3600 to 3200 cm^{-1} in the spectrum corresponding to SiO_2 ntbs (Figure 3a) can be assigned to the characteristic absorption of the O−H stretching. The peaks at 1100 cm^{-1} are because of the −Si−O−Si− stretching of the silica network, whereas the asymmetric stretching of Si−O−Si (νSi−O−Si) is obvious at 473 cm^{-1}. The stretching vibrations of Si−OH (νSi−OH) groups appear at about 810 cm^{-1}.[25] Figure 3b shows the FT-IR spectrum of the SrHA nrds. The typical bands of apatite can be seen in this figure. The absorption peaks at 1082 and 1017 cm^{-1} are ascribed to the asymmetric stretching vibrations of P−O, whereas the group of bands in the low-wavenumber range centered at 598 and 561 cm^{-1} is assigned to the bending vibrations of O−P−O in PO_4^{3-} groups. The bands at 3447 cm^{-1} arise out of the O−H stretching, and the two weak bands observed at 1413 and 1435 cm^{-1} can be attributed to the carbon-related impurities, due to the presence of CO_2 in the aqueous solution or air during the process of measuring.[26]

DOI: 10.1021/acsomega.7b01756
ACS Omega 2018, 3, 1509−1521

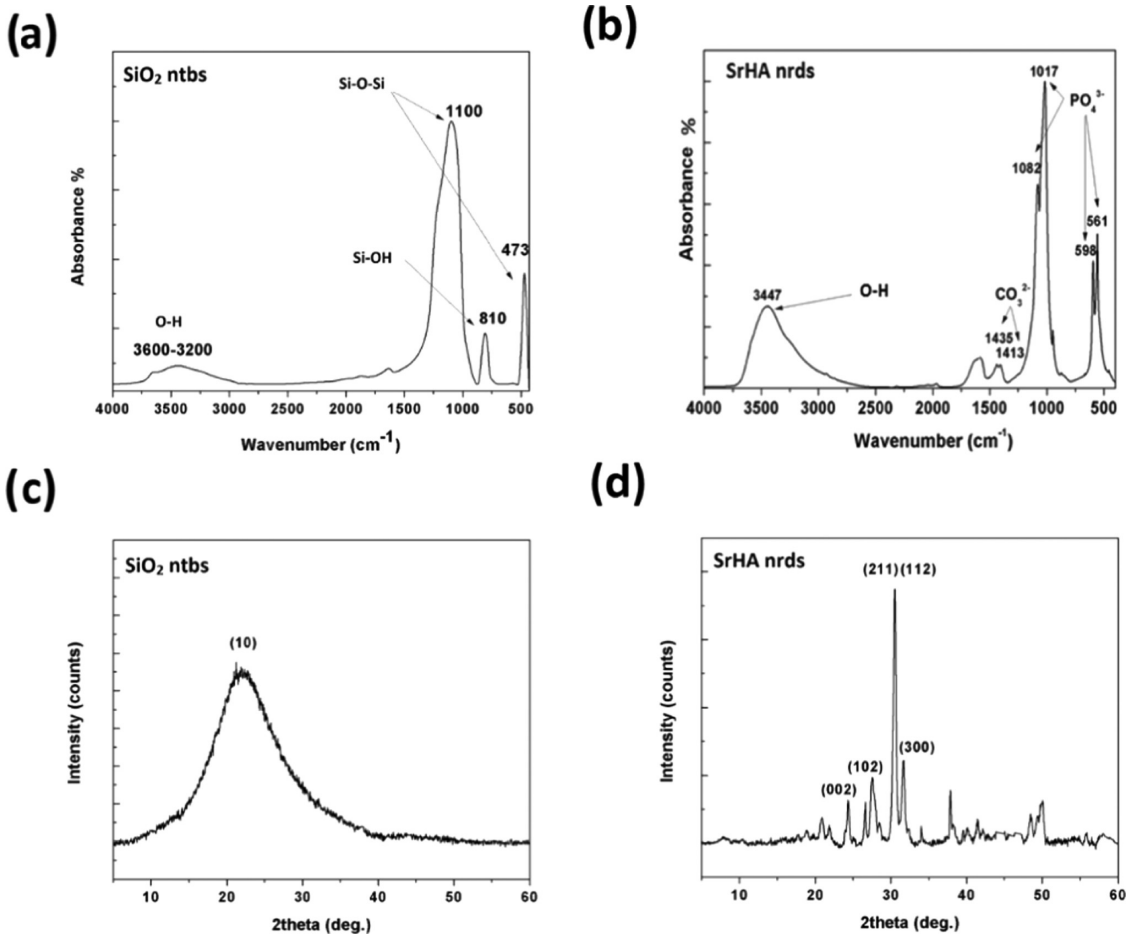

Figure 3. a, b) FT-IR spectra and (c, d) X-ray diffraction (XRD) patterns of SiO_2 ntbs and SrHA nrds.

Powder XRD pattern of SiO_2 ntbs in Figure 3c shows that only one broad peak appears at about 2θ 23−24°, indicating that the silica framework is amorphous. In contrast, the peaks appearing in the XRD pattern of the SrHA nrds are strong and narrow, indicating that the as-prepared sample was well crystallized despite the fact that relatively moderate reaction conditions were used (Figure 3d). The diffraction peaks at 2θ 26.8, 24.6, 30.6, and 31.8° are characteristic of the polycrystalline nature indexed to the (102), (002), (211), and (112) planes of the hexagonal phase of $Sr_{10}(PO_4)_6(OH)_2$, respectively, demonstrating that the pure SrHA crystals were obtained.[27]

2.2. Characterization of CAM-Loaded SrHA nrds and CAM-Loaded SiO_2 ntbs. As confirmed by TEM observations, one-dimensional SiO_2 ntbs display structures that provide unique characteristics such a very uniform diameter and being open at both ends. Chen and co-workers were the first to report silica tubular-structured materials as biomolecule carriers.[28] In their study, it was proved that the monkey kidney cells exhibited green fluorescence protein (GFP) expression when nanotubes filled with the gene encoding GFP entered these cells. Essentially, the fluorescent properties of the nanotubes allowed visualizing their localization in the living cells. Table 1 displays the drug loading and entrapment efficiency of SiO_2 ntbs prepared using the sol−gel methods. The least chloramphenicol (CAM) antibacterial drug loading (4.88 ± 0.48%) and entrapment efficiency (3.14 ± 0.23%) was found in SiO_2 ntbs prepared using the sol−gel method. These observations demonstrate a new potential application of nanotubes in biomolecule delivery because, except for DNA or drug molecules, RNA, proteins, antibiotics, and other biomolecules could also be loaded into the nanotubes. Moreover, the size of the nanotubes could be controlled and adjusted according to the size and the amount of cargo molecules, as a smaller nanovector might increase the transfection or delivery efficiency.[29]

Table 1. Drug Loading and Encapsulation Efficiency of SrHA nrds and SiO_2 ntbs

sample[a]	drug loading (%)	encapsulation efficiency (%)
CAM-loaded SrHA nrds	6.27 ± 0.74	4.03 ± 0.32
CAM-loaded SiO_2 ntbs	4.88 ± 0.48	3.14 ± 0.23

[a]Three measurements per condition were obtained. Standard deviation (σ) has been calculated using the following formula: $\sigma = \sqrt{[\sum (x - \text{mean}) \wedge 2/N}$.

Slightly increased drug loading (6.27 ± 0.74%) and entrapment efficiency (4.03 ± 0.32%) were obtained in the case of mesoporous SrHA nrds (Table 1). In a previous study, we found that SrHAp nrds have a surface area of 45 m^2/g and a pore volume of 0.485 cm^3/g.[26] Although these results show that SrHAp nrds have relatively low surface area compared to that of other aluminosilicate minerals, such as zeolites (500−1000 m^2/g), they also demonstrate that they possess big meso- and macropores with an average size of about 15−200 nm and high external surface area. Indeed, it has been previously proven that

DOI: 10.1021/acsomega.7b01756
ACS Omega 2018, 3, 1509−1521

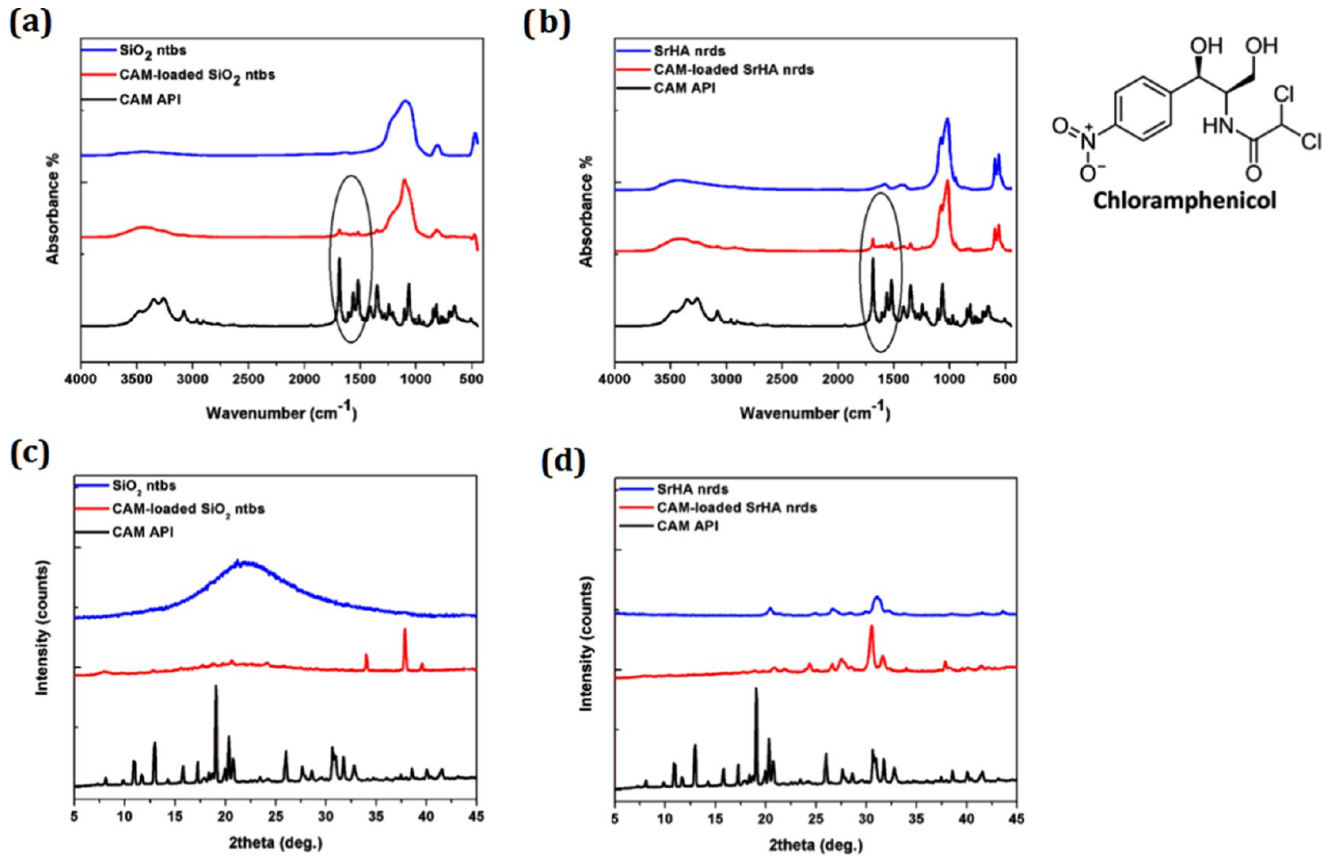

Figure 4. a, b) FT-IR spectra and (c, d) XRD patterns of SiO_2 ntbs and SrHA nrds before and after CAM loading.

mesoporous hydroxyapatite is an ideal drug carrier owing to its bioactvity, biocompatibility, porous structure, and numerous phosphate groups. Concerning SrHA nrds, they are well known to be used for antibiotic and anticancer drug delivery or for adsorbing heavy metals from wastewater.[26] From the present study, it can be concluded that the tunable mesopore structure of SrHA nrds allows the incorporation of CAM drug molecules.

FT-IR spectra were analyzed to investigate whether there are any chemical interactions between the chloramphenicol active pharmaceutical ingredient (CAM API) drug and the nanoparticles. FT-IR spectra of CAM API, SiO_2 ntbs, and SrHA nrds (before and after drug loading) are shown in Figure 4a,b. The characteristic infrared peaks of CAM API indicate O−H, N−H, and C−H stretching vibrations between 2900 and 3500 cm^{-1}.[30] The characteristic sharp peak corresponding to C═O of the carbonyl group appears at 1683 cm^{-1}, whereas the nitrogen dioxide (NO_2) group shows an intense double peak between 1400 and 1550 cm^{-1}, assigned to the N═O stretching vibrational mode. For the drug-loaded forms, C═O and N═O peaks of chloramphenicol can be observed, suggesting that chloramphenicol slightly interacted with the surface of the NPs and that it was not completely entrapped in their cavities.[31]

Furthermore, almost all of the peaks appearing in the spectra of CAM-loaded SrHA nrds and CAM-loaded SiO_2 ntbs were the same as those of the pure SrHA nrds and SiO_2 ntbs, with no changes observed in the intensities. (Figure 4a,b). This seems to indicate the absence of chemical interaction between the NPs and the chloramphenicol drug. Interestingly, end functionalization of SrHA nrds and SiO_2 ntbs may be able to control drug release, resulting in their wide range of applications in controlled drug and gene delivery; also, their distinctive inner and outer surfaces can be differentially functionalized, making silica nanotubes ideal multifunctional nanostructure candidates for biomedical applications in various areas, such as biosensing, bioseparation, and biocatalysis.[24,29]

XRD measurements were also performed in CAM API and in CAM-loaded NPs to identify the physical state of the drug. As can be seen from the XRD data (Figure 4c,d), the XRD pattern of pure CAM shows many sharp diffraction peaks at 2θ 10.76, 12.82, 18.90, 25.88, and 31.62°. Because the main characteristic peaks of CAM were not recorded in the drug-loaded forms, we can assume that it was entrapped in the amorphous state, which is very normal when inorganic particles with high surface area of 100−1000 m^2/g are used for drug loading.[31] However, the absence of the main characteristic peaks of CAM could also be due to the low drug loading.

Nanoparticles provide a versatile platform in designing materials for antimicrobial therapy. NP-based antimicrobial agents can be readily used for ex vivo applications such as sterilizers for surfaces and devices. Moreover, excellent biofilm penetration enhances their activity toward a range of biofilm-based infections. The most accessible target in the near future includes the topical applications of NP-based systems for wound healing.[7] Here, tunable surface functionality and multivalence of SrHA nrds and SiO_2 ntbs make them promising antimicrobial agents, whereas localized delivery of the CAM antibiotic increases the therapeutic efficacy of CAM-loaded-SrHA nrds and CAM-loaded-SiO_2 ntbs.[10,32,33]

2.3. Antibacterial Activity of CAM-Loaded-SrHA ntbs and CAM-Loaded-SiO_2 ntbs. The antibacterial activity of CAM-loaded-SrHA ntbs and CAM-loaded-SiO_2 ntbs was determined using the minimum inhibitory concentration

DOI: 10.1021/acsomega.7b01756
ACS Omega 2018, 3, 1509−1521

method against four bacteria: *Escherichia coli*, *Bacillus subtilis*, *Benthesicymus cereus*, and *Staphylococcus aureus*. SrHA ntbs and SiO_2 ntbs were also used as negative controls. Both CAM-loaded ntbs exhibited dose-dependent antibacterial activity against all of the bacteria tested. They were most effective against *E. coli* with an IC_{50} value of 51.37 μg/mL for CAM-loaded-SrHA ntbs and 57.32 μg/mL for CAM-loaded-SiO_2 ntbs (Table 2). The observed antibacterial activity of CAM-loaded-SrHA ntbs seems to be slightly higher than that of CAM-loaded-SiO_2 ntbs against *E. coli*, *B. subtilis*, and *S. aureus*, whereas their difference was higher in the case of *B. cereus*.

Table 2. Antibacterial Activity of SrHA nrds, SiO_2 ntbs, CAM-Loaded-SrHA ntbs, and CAM-Loaded-SiO_2 ntbs

IC_{50} (μg/mL)	*E. coli*	*B. subtilis*	*B. cereus*	*S. aureus*
CAM-loaded SrHA nrds	51.37	162.44	83.72	119.02
CAM-loaded SiO_2 ntbs	57.32	167.50	123.43	131.10
SrHA ntbs	140.13	223.51	143.94	187.83
SiO_2 ntbs	310.92	209.03	224.42	209.73

However, even if the biocompatibility of silica-based and hydroxyapatite-based nanoparticles makes them especially ideal carriers for applications associated with the human body, further studies at the fundamental, biological, and pharmacological levels are required to enable systemic administration of these antimicrobials.[7]

2.4. Black Silicon and Hierarchical Surface Design by Means of Thermal NIL. Although the NIL processes are mainly used to produce high-aspect-ratio silicon surfaces for designing semiconductors and photovoltaic materials, very recently they have been used in some biological applications to produce features ranging from tens of micrometers down to hundreds of nanometers.[34−36] In the present study, the formation of nano- and hierarchical (micro and nano) structures on the surface of PLLA has been investigated by means of thermal NIL to produce PLLA nanocomposite surfaces with antibacterial properties. As it can be seen in Figure 5, random cone- and needle-shaped nanostructures, 1−2 μm tall and 300−500 nm in diameter, were faithfully replicated on the surface of PLLA by thermal NIL for the first time. Because of the high aspect ratios, the etched nanostructure sometimes is antireflective and turns black after the etching and is therefore termed as black silicon (BS).[4] Interestingly, antireflective nanostructures, which have been inspired by objects in nature, such as insect wings and the surfaces of insect eyes, have also the potential to generating a mechanical bactericidal effect, killing both Gram-negative and Gram-positive bacteria at high rates.[37]

Moreover, to increase the surface roughness and to decrease the solid−liquid contact function, we tried to combine micro-

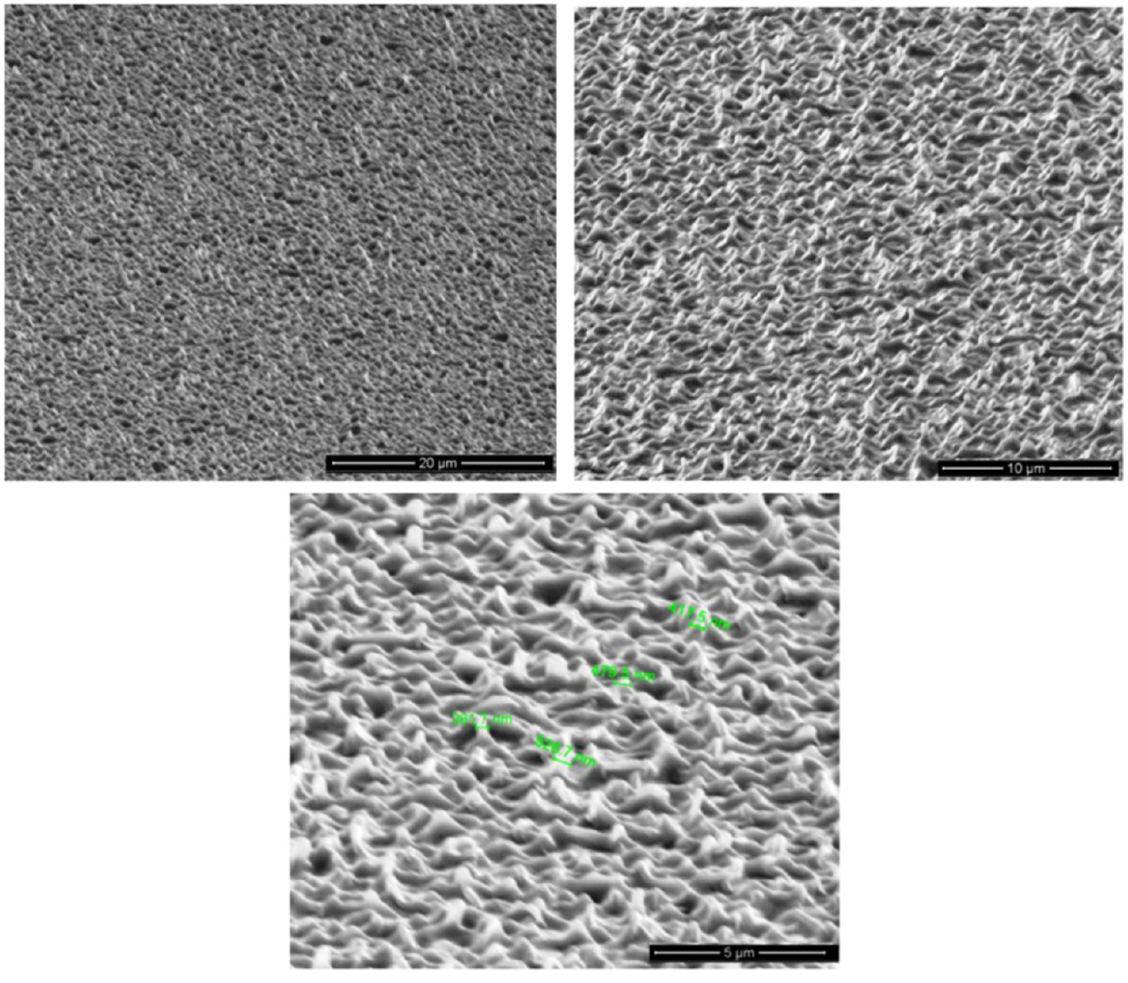

Figure 5. Scanning electron microscopy (SEM) images of the black silicon nanostructured PLLA surface at different magnifications.

DOI: 10.1021/acsomega.7b01756
ACS Omega 2018, 3, 1509−1521

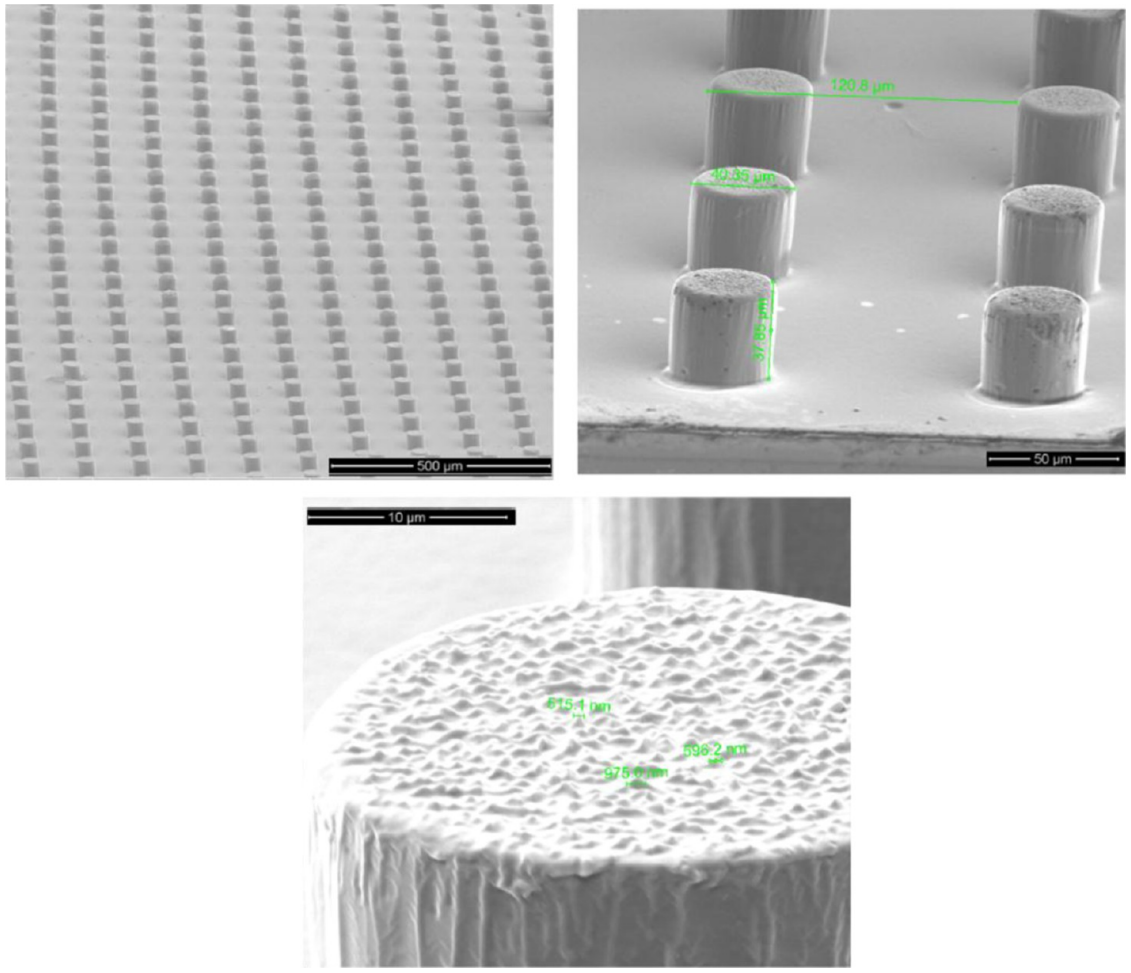

Figure 6. Tilted SEM images of the 3D hierarchical domains on the surface of PLLA (black silicon nanostructures on micropillars) at different magnifications.

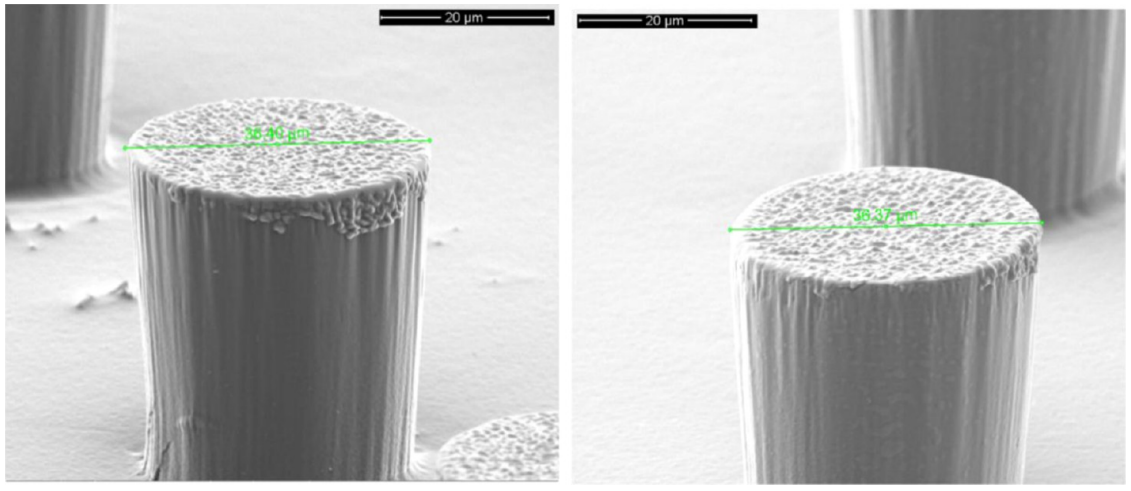

Figure 7. Left: SEM observation of one micropillar on the surface of PLLA/CAM-loaded SrHA nrds 1%. Right: SEM observation of one micropillar on the surface of PLLA/CAM-loaded SiO_2 ntbs 1%.

with nanoscale patterning.[5] In Figure 6, we present the novel three-dimensional (3D) hierarchical domains on the surface of PLLA. It can be seen that cylindrical micropillars with 40 μm width or diameter and 40 μm height decorated with BS nanostructures on the top surface were successfully fabricated. Given the growing interest in the development of biomimetic antibacterial surfaces, these results may be useful, offering an alternative geometry for production of nanoscale antibacterial surfaces.

In addition, neither CAM-free nor CAM-loaded SrHA nrds and SiO_2 ntbs affected the NIL process negatively because nice black silicon and hierarchical structures were obtained also for

DOI: 10.1021/acsomega.7b01756
ACS Omega 2018, 3, 1509−1521

the PLLA nanocomposite films. In Figure 7, the presence of the nanoparticles loaded with CAM and their good dispersion in the polymer matrix can be seen in the main body of the micropillars. The lack of agglomerates could be attributed to the spin-coating method that was used for the preparation of the PLLA nanocomposite thin films.

To quantify the bactericidal properties of the black silicon and the 3D hierarchical surfaces, two species of bacteria were incubated on each surface for periods up to 24 h and the bacterial viability was monitored. The bacterial species examined represented the major prokaryotic taxa and included Gram-negative *E. coli* and Gram-positive *S. aureus*. We calculated the ratio of cell density on each patterned surface with respect to the corresponding upatterned surface (control sample). As shown in Figures 8 and 9, we consistently

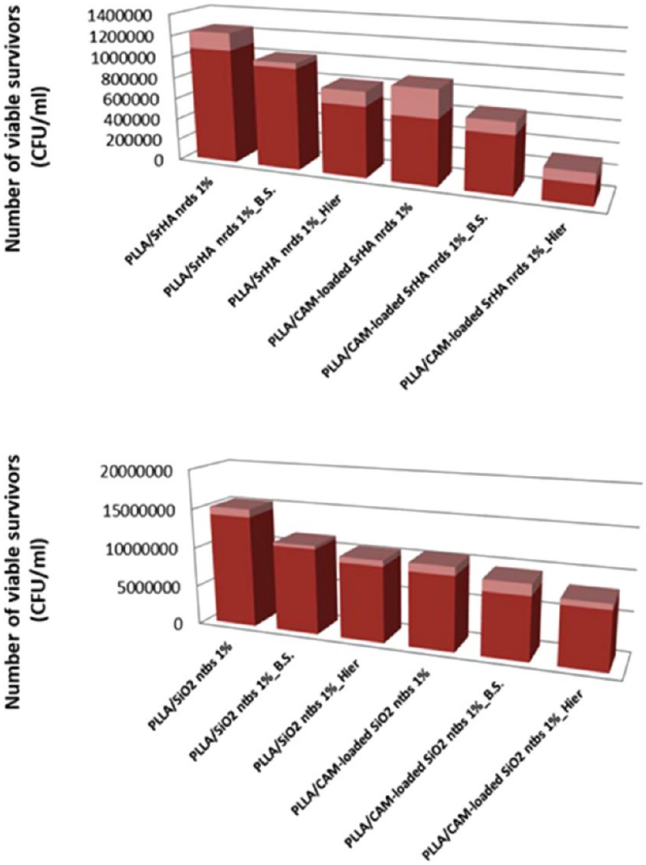

Figure 8. Antibacterial activity against *E. coli* after 24 h of incubation.

measured lower cell densities on the patterned surfaces (PLLA or SrHA nrds and PLLA or SiO_2 ntbs) than on the flat surfaces (PLLA or SrHA nrds Hier PLLA or SiO_2 ntbs Hier). Additionally, the results plotted in Figures 8 and 9 clearly show that the cellular density depends on the surface geometry, as the hierarchical surfaces show a further decrease in cell density compared to that on the corresponding nanostructured black silicon surfaces.[38] These results are in good agreement with a previous study, in which bSi and dragonfly wing surfaces were effective not only against the Gram-negative *E. coli* cells but also against the Gram-positive *S. aureus* cells.[6,37]

In addition to the physical effects of nanostructures and micro- or nanostructures, the chemical effects, because of the presence of chloramphenicol in the case of PLLA/CAM-loaded SrHA nrds and PLLA/CAM-loaded SiO_2 ntbs samples, play

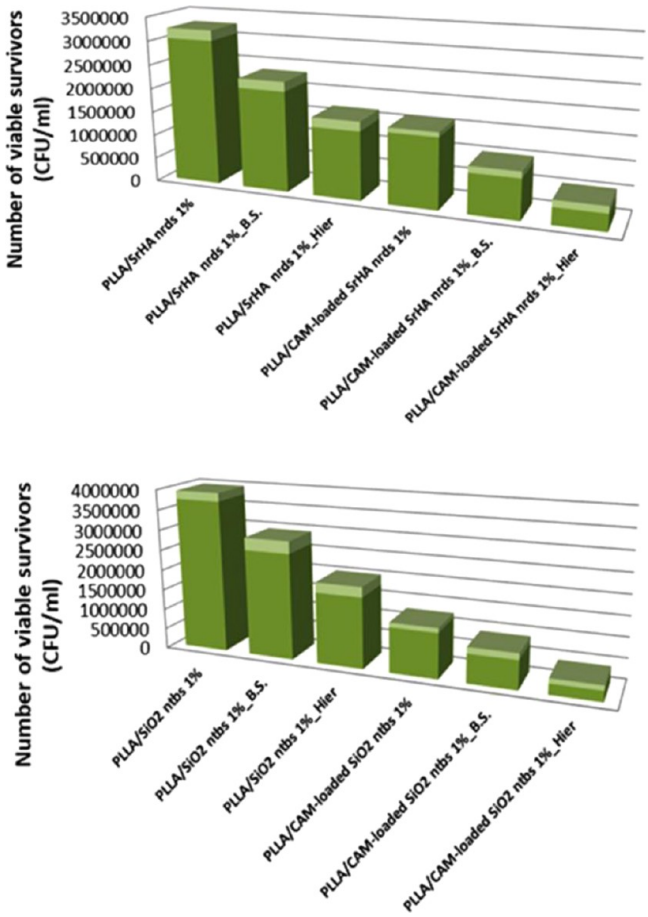

Figure 9. Antibacterial activity against *S. aureus* after 24 h of incubation.

important roles in conjunction with the physical ones on the bactericidal effects. Chloramphenicol enters the bacteria by an energy-dependent process. Its antibiotic activity is due to competitive inhibition for the binding of aminoacyl tRNA to the peptidyltransferase domain of the 50S subunit.[39] By incorporating a "smart" bacteria-triggered nano or micro-/nanostructure, a greater exposure of the antibiotic to the adhering bacteria was provided, and it led to an increase in the antibacterial efficiency of the PLLA/CAM-loaded SrHA nrds BS and PLLA/CAM-loaded SiO_2 ntbs BS samples compared to that of the unpatterned PLLA/CAM-loaded SrHA nrds and PLLA/CAM-loaded SiO_2 ntbs flat surfaces, respectively.[38] Furthermore, an additional advantage comes from the reduction of bacterial adhesion and an increase in their susceptibility to antibiotic when bacteria land on the 3D PLLA/CAM-loaded SrHA nrds Hier and PLLA/CAM-loaded SiO_2 ntbs Hier structures. The demonstrated strategy of a synergistic combination of advanced 3D nanostructuring and antibiotic nanoparticulated delivery holds a great promise for engineering of bacteria-resistant PLLA surfaces.

Viability staining was also coupled with SEM imaging after 24 h bacterial adhesion. We fixed the bacterial cells with glutaraldehyde (as mentioned in Section 2) before SEM imaging, which crosslinks the proteins, making the cell more resistant to changes under vacuum. The morphology and distribution of all of the cells that attached to the surface of the "flat" unpatterned PLLA and SrHA nrds 1 wt %, which acted as control surface, were found to be significantly different from

DOI: 10.1021/acsomega.7b01756
ACS Omega 2018, 3, 1509−1521

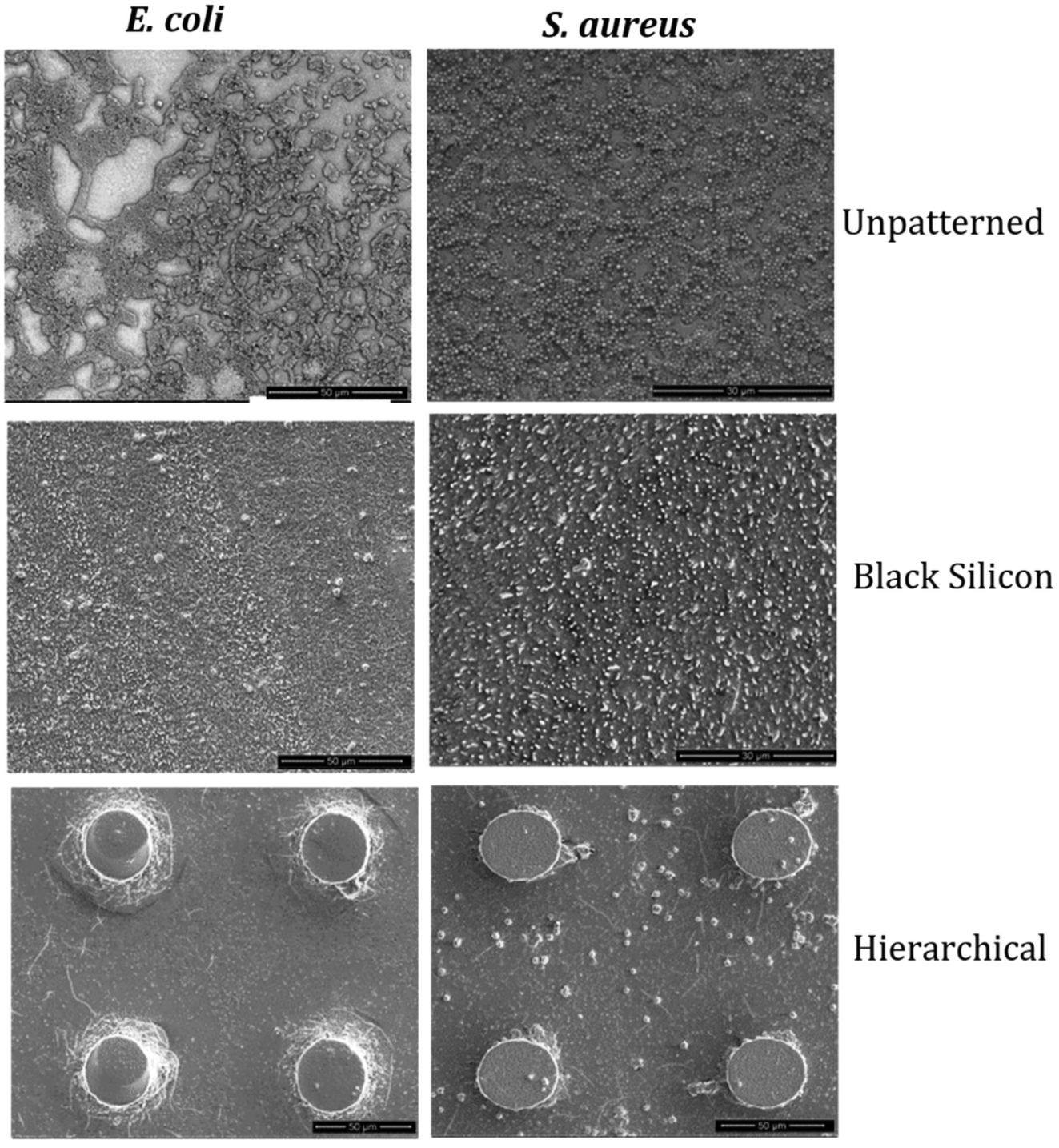

Figure 10. SEM analysis, the reference strain SEM observations of "rod-shaped" *E. coli* and "coccoid-shaped" *S. aureus* on flat unpatterned, black silicon, and hierarchical domains on the surface of the PLLA/CAM-loaded SrHA nrds 1% sample.

those of the cells attached to PLLA/CAM-loaded SrHA nrds 1 wt % BS and PLLA/CAM-loaded SrHA nrds 1 wt % Hier surfaces (Figure 10).

Rod-shaped *E. coli* and coccoid-shaped *S. aureus* cells adhered horizontally and appeared to remain in a healthy state (turgid) on the flat unpatterned surface. In contrast, on the black silicon and hierarchical surface, a proportion of the cells appeared to be flat and nonturgid.[40] Thus, the greater nonuniformity of the surface appeared to effectively damage a higher percentage of the bacterial cells, which is consistent with the results from the Live/Dead assays. Although on nano and micro-/nanostructures, bacteria appeared deflated as they stretched over several pillars, SEM observations did not explain the underlying mechanism behind the higher killing efficiency of the hierarchical surfaces, and further studies will be necessary to throw some light on this complex procedure.[3]

Nanomaterials that possess topographical features with high aspect ratios frequently display remarkable surface properties such as high hydrophobicity that is often related to cell attachment and biofilm formation.[4,41] This could also play, maybe, an important role in the antimicrobial properties of the prepared surfaces. To check this, in our study, water contact

DOI: 10.1021/acsomega.7b01756
ACS Omega 2018, 3, 1509−1521

Table 3. Water Contact Angle Measurements

sample	water contact angle (degrees)		
	unpatterned	black silicon	hierarchical
PLLA/SrHA nrds 1%	94 ± 2	113 ± 3	128 ± 3
PLLA/CAM-loaded SrHA nrds 1%	96 ± 1	117 ± 1	132 ± 2
PLLA/SiO_2 ntbs 1%	98 ± 2	134 ± 3	146 ± 1
PLLA/CAM-loaded SiO_2 ntbs 1%	100 ± 1	138 ± 2	147 ± 2

angle measurements have been also carried out. From the results presented in Table 3, it is clear that the hierarchical surfaces were highly hydrophobic, whereas the black silicon surfaces were relatively lower in hydrophobicity. These results indicate that it is difficult to achieve the superhydrophobicity property because of nanoscale topography alone and hierarchical roughness is essential to impart these properties.[42] Although our findings suggest that highly hydrophobic surfaces do inhibit the attachment of bacterial cells,[6] many studies have also shown that there is no direct relationship between superhydrophobicity and antibacterial activity.[43] However, from our results, it seems that the high hydrophobicity of hierarchical structures could also be because of their higher antimicrobial properties.

3. CONCLUSIONS

We have demonstrated that strategies that confine antibacterial property to PLLA, by encapsulating chloramphenicol-loaded nanoparticles and by imprinting nano- and micro-/nano-domains on the surface of nanocomposite PLLA films by NIL, are very promising. The results of this work indicate that both *E. coli* and *S. aureus* cells attached onto the nanostructured and micro-/nanostructured surfaces to a smaller extent compared to that on the unpatterned smooth samples. The hierarchical fabricated PLLA/CAM-loaded SrHA nrds 1% and PLLA/CAM-loaded SiO_2 ntbs 1% surfaces were particularly effective against the pathogens, as the 3D surface allowed a greater exposure of the antibiotic to the adhering bacteria and increased the antibacterial efficiency. It is thus suggested that repelling the bacteria from the surface and at the same time killing the ones that managed to adhere to the patterned surface by the nanoparticle antibiotic delivery platforms could be the most effective strategy for antibacterial surface design. However, this scientific field is new and much of the important work is still in the proof-of-concept stage.

4. MATERIALS AND METHODS

4.1. Materials. Strontium nitrate [$Sr(NO_3)_2$] (≥99%), ammonium phosphate dibasic [$(NH_4)_2HPO_4$] (≥98%), and trisodium citrate dehydrate [$C_6H_5Na_3O_7{\cdot}2H_2O$], (labeled as Cit^{3-}) (6132-04-3) (≥99%) were supplied by Sigma Aldrich Chemical Co. (Chemie GmbH, Germany). Cetyltrimethylammonium bromide (labeled as CTAB) (≥99%) was purchased from Panreac Quimicha (Panreac Quimica S.L.U., Spain). Citric acid [$HOC(COOH)(CH_2COOH)_2$] and tetra-*ortho*-silicate [$Si(OC_2H_5)_4$] (labeled as TEOS) were purchased from Sigma Aldrich Chemical Co. (Chemie GmbH, Germany). Poly(L-lactic acid) (PLLA) (M_w 63.090 g/mol), under the trade name Ingeo Biopolymer 3052D, was kindly supplied by Plastika Kritis S.A. Chloramphenicol API ($C_{11}H_{12}C_{l2}N_2O_5$), as a wide-spectrum antibiotic, was kindly provided by Pharmathen Industrial S.A. Silicon wafers [Prime CZ-Si wafer 4 in., thickness 525 ± 25 μm, (100), 1-side polished, p-type (boron) total thickness variation < 10 μm] were supplied by MicroChemicals. Chloroform ($CHCl_3$) (99.5%) was obtained from Chem-Lab NV. All of the other materials and solvents used in the analytical methods were of analytical grade.

4.2. Synthesis of SrHA nrds and SiO_2 ntbs. Single SiO_2 nanotubes (SiO_2 ntbs) were synthesized by modifying a previously reported sol−gel process.[17] Ethanol, water, TEOS, and ammonia were used as chemical sources. Citric acid (CA) monohydrate was also employed as a structural modifier. In a typical synthetic procedure, 6.0 mL of TEOS was added to the mixed solution of 0.7 mL of H_2O and 30 mL of EtOH. Then, 12 mL of NH_4OH (28% aqueous solution) containing 0.18 g of CA monohydrate was added dropwise into the homogenous solution for 2 h under vigorous magnetic stirring. The as-obtained mixture was transferred into a Teflon bottle (80 mL), held in a stainless steel autoclave, sealed, and maintained at 200 °C for 24 h. As the autoclave cooled to room temperature naturally, the precipitate was washed centrifugally with distilled water and dried in an oven at 75 °C.

To synthesize SrHA nrds, we followed a previously described hydrothermal process involving the autoclave treatment of $Sr(NO_3)_2$ (3 mmol), CTAB (0.5 g), ammonia solution (NH_4OH) (10 mL), trisodium citrate (6 mmol), and $(NH_4)_2HPO_4$ (2 mmol).[18]

4.3. Drug Loading of SrHA nrds and SiO_2 ntbs. Drug loading of SiO_2 ntbs and SrHA nrds was performed by mixing, in the dark and under a nitrogen atmosphere, 50 mg of SrHA nrds or SiO_2 ntbs with aqueous solutions of chloramphenicol of selected concentration for 24 h to achieve an initial concentration of 150 μg/mg of nanoparticles. The chloramphenicol-loaded formulations, CAM-loaded SiO_2 ntbs and CAM-loaded SrHA nrds, were filtered, washed with 25 mL of water to remove the unloaded drug, and dried at room temperature.

4.4. Characterization of SrHA nrds and SiO_2 ntbs before and after Drug Loading. The morphology of the as-synthesized nanoparticles was studied using transmission electron microscopy (TEM). TEM imaging of SiO_2 ntbs was conducted using JEOL JEM-1400PLUS (40−120 kV) equipped with a GATAN US1000 charge-coupled device camera. An aliquot of 3.5 μL of each sample was deposited on a carbon film, 400 mesh copper (50/pk) grid, and left to evaporate at room temperature. Bright field transmission electron microscopy (TEM) images of SrHA nrds were acquired using a FEI Tecnai G2 microscope operated at 200 kV. Samples adequate for transmission electron microscopy were prepared by drop-casting the ethanol solution containing the particles on holey, carbon-coated copper grids.

To evaluate the chemical composition and the crystal structure of SrHA nrds and SiO_2 ntbs before and after drug loading, the as-synthesized nanoparticles and the CAM-loaded formulations were examined using Fourier transform infrared spectroscopy (FT-IR) and X-ray diffractometry (XRD). FT-IR spectra were obtained using a Perkin−Elmer FT-IR spectrometer, model Spectrum One, in absorbance mode, in the

DOI: 10.1021/acsomega.7b01756
ACS Omega 2018, 3, 1509−1521

spectral region of 400−4000 cm^{-1}, using a resolution of 4 cm^{-1} and 64 co-added scans. XRD patterns of the samples were collected using a MiniFlex II XRD system from Rigaku Co. X-ray diffraction measurements were carried out over the range 2θ from 5 to 30°, at steps of 0.05° and counting time of 5.

The drug-loading content and encapsulation efficiency of CAM-loaded formulations were determined indirectly by calculating spectrophotometrically the free drug in the combined filtrate and washing waters normalized at 25 mL, using a calibration curve. The calibration curve was created by diluting a stock aqueous solution of 400 ppm CAM to concentrations of 1, 10, 20, 40, 60, 80, and 100 ppm and then measuring the UV−vis absorbance at 278 nm. The following equations were applied to calculate the drug-loading content and encapsulation efficiency

$$\text{drug loading (\%)} = \frac{(\text{weight of drug in nanoparticles})}{(\text{weight of nanoparticles})} \times 100 \quad (1)$$

$$\text{entrapment efficiency (\%)} = \frac{(\text{weight of drug in nanoparticles})}{(\text{initial weight of drug})} \times 100 \quad (2)$$

Moreover, screening of the antibacterial activity of CAM-free and CAM-loaded nanoparticles was performed by determining the half-minimal inhibitory concentration (IC_{50}) [against *E. coli* (BL21), *B. subtilis* (ATCC 6633), *B. cereus* (ATCC 11778), and *S. aureus* (ATCC 25923), according to the method described recently by Varna et al.[44]].

4.5. Preparation of PLLA Nanocomposite Thin Films by Spin-Coating. Nanocomposites based on PLLA matrix were prepared according to the following procedure. First, PLLA was dissolved in chloroform to form a 10 wt % solution using magnetic stirring for 2 h at room temperature. At the same time, SrHA nrds, SiO_2 ntbs, CAM-loaded SrHA nrds, and CAM-loaded SiO_2 ntbs were weighted to achieve the desired final concentration (1 wt % on the basis of the weight of the composite material) and dispersed separately using magnetic stirring for 2 h and ultrasonication for 20 min. In the second step, both the polymer solution and the suspensions of the nanoparticles were mixed, stirred (2 h), and sonicated (15 min) to form nanocomposites with 1% weight fraction. The produced nanocomposite PLLA films were spin-coated on silicon substrates, cut into 2 cm × 2 cm square-pieces. Several coating speeds were tested to achieve the desired thickness, which was dependent on the used featured height. Before spin-coating, our Si wafers were O_2 plasma-treated (O_2 flow = 50 sccm, N_2 = 50 sccm, pressure = 100 mTorr, and power = 50 W) to enhance the polymer adherence and to eliminate any organic residuals that the samples might had.

4.6. Patterning of PLLA Nanocomposite Thin Films by Thermal Nanoimprint Lithography. Before the thermal NIL step, a hot-plate-induced soft bake was performed at 100 °C for 15 min to ensure that no solvent remained in the polymer nanocomposites. During our experimental work, thermal NIL was performed using a commercial desktop 4 in. CNI tool obtained from NIL Technology Aps. During the NIL process, polydimethylsiloxane (PDMS) stamps, which provided the suitable flexibility, were prepared to achieve a soft release and a successful replication. Apparently, the use of the PDMS stamps at relatively high temperatures while maintaining the pressure at low values allowed us to replicate hierarchical topographies in one step. The nanocomposite substrate and the stamp were heated to 170 °C, and a pressure of 5 bars was applied for 20 min. After cooling to below 40 °C, the stamp and the biopolymer were separated.

4.7. Characterization of PLLA Nanocomposite Thin Films before and after Patterning. The microstructure and the surface morphology were observed using a field emission scanning electron microscope (SEM) (FEI Quanta 650 FEG). A modern droplet shape analysis instrument from Kruss was used to measure the wetting behavior of our produced (micro- and/or nanostructured) surfaces. A water droplet (smaller than the capillary length) was gently placed on the surface using a needle, and its contact angle values were measured using the sessile droplet method. A camera and a computer with commercial software were used to measure the static contact angle after the needle was removed.

The antibacterial activity of PLLA nanocomposite films, before and after patterning, was evaluated according to ISO 207043:2007. Bacterial strains of *E. coli* (BL21) and *S. aureus* (ATCC 25923) were used as the model Gram-negative and Gram-positive bacteria, respectively. Cells were grown in 100 mL of sterile nutrient broth (Luria-Bertani broth) at 150 rpm and 37 °C. The cells were collected at the logarithmic stage of growth, and the concentration of the suspensions was adjusted to OD_{600} (optical density at 600 nm) value of 0.5 in 25 mM phosphate-buffered saline (PBS, Sigma) solution before incubation with the nanostructured surface measuring 0.5 cm × 0.5 cm in area. The as-received PLLA-coated Si wafer without nanostructures of the same dimension was used as the control. In addition, a well without a Si wafer served as an additional control. The nanostructured and control surfaces were immersed in 1 mL of the bacterial suspension in a 24-well plate. The growth of the adhered cells on the nanostructured and control silicon surfaces was identified at different time intervals of 6, 12, and 24 h by measuring the absorbance values at OD_{600} in triplicates. In addition, 100 μL of the cell suspensions after 1 h of incubation with the nanostructured and control surfaces was taken and diluted 10-folds. Each of the diluted suspensions was spread onto three nutrient agar plates. Resulting colonies were then counted after 24 h of incubation at 37 °C, and the number of colony-forming units per milliliter was calculated. To assess the morphology of the adherent bacterial cells after 1 h, the nanostructured and control surfaces were washed with fresh PBS and fixed with 2.5% glutaraldehyde for 30 min. The samples were sputtered with gold before imaging by SEM.[42]

AUTHOR INFORMATION

Corresponding Author

*E-mail: dbic@chem.auth.gr.

ORCID

Ariadna Fernández: 0000-0001-7559-2037

Clivia M. Sotomayor Torres: 0000-0001-9986-2716

Dimitrios N. Bikiaris: 0000-0001-8458-4952

Notes

The authors declare no competing financial interest.

ACKNOWLEDGMENTS

The authors wish to thank Prof. G. Van Tendeloo and Dr. M. Filippousi (EMAT University of Antwerp, Belgium) for bright

DOI: 10.1021/acsomega.7b01756
ACS Omega 2018, 3, 1509−1521

field TEM imaging of SrHA nrds and Dr. Eleftheria Diamanti (Postdoctoral Researcher, ELKARTEK fellow CIC nanoGUNE Consolider, Donostia/San Sebastián, Spain) for acquiring TEM images of SiO_2 ntbs. ICN_2 acknowledges support from the Severo Ochoa Program (MINECO, Grant SEV-2013-0295) and funding from the CERCA Programme/Generalitat de Catalunya.

REFERENCES

(1) Hasan, J.; Chatterjee, K. Recent advances in engineering topography mediated antibacterial surfaces. *Nanoscale* **2015**, *7*, 15568−15575.
(2) Ren, W.; Cheng, W.; Wang, G.; Liu, Y. Developments in antimicrobial polymers. *J. Polym. Sci., Part A: Polym. Chem.* **2017**, *55*, 632−639.
(3) Jäger, M.; Jennissen, H. P.; Dittrich, F.; Fischer, A.; Köhling, H. L. Antimicrobial and osseointegration properties of nanostructured titanium orthopaedic implants. *Materials* **2017**, *10*, No. 1302.
(4) Kim, S.; Jung, U. T.; Kim, S. K.; Lee, J. H.; Choi, H. S.; Kim, C. S.; Jeong, M. Y. Nanostructured multifunctional surface with antireflective and antimicrobial characteristics. *ACS Appl. Mater. Interfaces* **2015**, *7*, 326−331.
(5) May, R. M.; Magin, C. M.; Mann, E. E.; Drinker, M. C.; Fraser, J. C.; Siedlecki, C. A.; Brennan, A. B.; Reddy, S. T. An engineered micropattern to reduce bacterial colonization, platelet adhesion and fibrin sheath formation for improved biocompatibility of central venous catheters. *Clin. Transl. Med.* **2015**, *4*, 9.
(6) Tripathy, A.; Sen, P.; Su, B.; Briscoe, W. H. Natural and bioinspired nanostructured bactericidal surfaces. *Adv. Colloid Interface Sci.* **2017**, *248*, 85−104.
(7) Gupta, A.; Landis, R. F.; Rotello, V. M. Nanoparticle-based antimicrobials: surface functionality is critical. *F1000Research* **2016**, *5*, No. 364.
(8) Miller, K. P.; Wang, L.; Benicewicz, B. C.; Decho, A. W. Inorganic nanoparticles engineered to attack bacteria. *Chem. Soc. Rev.* **2015**, *44*, 7787−7807.
(9) Ladavière, C.; Gref, R. Toward an optimized treatment of intracellular bacterial infections: input of nanoparticulate drug delivery systems. *Nanomedicine* **2015**, *10*, 3033−3055.
(10) Yacoby, I.; Bar, H.; Benhar, I. Targeted drug-carrying bacteriophages as antibacterial nanomedicines. *Antimicrob. Agents Chemother.* **2007**, *51*, 2156−2163.
(11) Geng, Z.; Cui, Z.; Li, Z.; Zhu, S.; Liang, Y.; Liu, Y.; Li, X.; He, X.; et al. Strontium incorporation to optimize the antibacterial and biological characteristics of silver-substituted hydroxyapatite coating. *Mater. Sci. Eng., C* **2016**, *58*, 467−477.
(12) Swetha, M.; Sahithi, K.; Moorthi, A.; Saranya, N.; Saravanan, S.; Ramasamy, K.; Srinivasan, N.; Selvamurugan, N. Synthesis, characterization, and antimicrobial activity of nano-hydroxyapatite-zinc for bone tissue engineering applications. *J. Nanosci. Nanotechnol.* **2012**, *12*, 167−172.
(13) Beltrán-Osuna, A. A.; Perilla, J. E. Colloidal and spherical mesoporous silica particles: synthesis and new technologies for delivery applications. *J. Sol-Gel Sci. Technol.* **2016**, *77*, 480−496.
(14) Dickson, M. N.; Liang, E. I.; Rodriguez, L. A.; Vollereaux, N.; Yee, A. F. Nanopatterned polymer surfaces with bactericidal properties nanopatterned polymer surfaces with bactericidal properties. *Biointerphases* **2015**, *10*, No. 021010.
(15) Turalija, M.; Bischof, S.; Budimir, A.; Gaan, S. Antimicrobial PLA films from environment friendly additives. *Composites, Part B* **2016**, *102*, 94−99.
(16) Sousa, C.; Rodrigues, D.; Oliveira, R.; Song, W.; Mano, J. F.; Azeredo, J. Superhydrophobic poly (L-lactic acid) surface as potential bacterial colonization substrate. *AMB Express* **2011**, *1*, 34.
(17) Wang, L.; Tomura, S.; Ohashi, F.; Maeda, M.; Suzuki, M.; Inukai, K. Synthesis of single silica nanotubes in the presence of citric acid. *J. Mater. Chem.* **2001**, *11*, 1465−1468.
(18) Zhang, C.; Li, C.; Huang, S.; Hou, Z.; Cheng, Z.; Yang, P.; Peng, C.; Lin, J. Self-activated luminescent and mesoporous strontium hydroxyapatite nanorods for drug delivery. *Biomaterials* **2010**, *31*, 3374−3383.
(19) Yang, X.; Tang, H.; Cao, K.; Song, H.; Sheng, W.; Wu, Q. Templated-assisted one-dimensional silica nanotubes: synthesis and applications. *J. Mater. Chem.* **2011**, *21*, 6122−6135.
(20) Adachi, M.; Harada, T.; Harada, M. Formation of huge length silica nanotubes by a templating mechanism in the laurylamine/tetraethoxysilane system. *Langmuir* **1999**, *15*, 7097−7100.
(21) Anglin, E. J.; Cheng, L.; Freeman, W. R.; Sailor, M. J. Porous silicon in drug delivery devices and materials. *Adv. Drug Delivery Rev.* **2008**, *60*, 1266−1277.
(22) Christenson, E. M.; Anseth, K. S.; van den Beucken, J. J.; Chan, C. K.; Ercan, B.; Jansen, J. A.; Laurencin, C. T.; Li, W.; Murugan, R.; Nair, L. S.; et al. Nanobiomaterial applications in orthopedics. *J. Orthop. Res.* **2007**, *25*, 11−22.
(23) Bilton, M.; Milne, S. J.; Brown, A. P. Comparison of Hydrothermal and Sol-gel synthesis of nano-particulate hydroxyapatite by characterisation at the bulk and particle level. *Open J. Inorg. Non-Met. Mater.* **2012**, *2*, 1−10.
(24) Chen, X.; Cai, Q.; Sun, L. H.; Zhang, W.; Jiang, X. Y. Synthesis of Novel thiol-functionalized mesoporous silica nanorods and their sorbent properties on heavy metals. *Front. Mater. Sci.* **2012**, *6*, 278−282.
(25) Nerantzaki, M.; et al. Novel Poly(butylene Succinate) Nanocomposites containing strontium hydroxyapatite nanorods with enhanced osteoconductivity for tissue engineering applications. *eXPRESS Polym. Lett.* **2015**, *9*, 773−789.
(26) Filippousi, M.; Siafaka, P. I.; Amanatiadou, E. P.; Nanaki, S. G.; Neratzaki, M.; Bikiaris, D. N.; Vizirianakis, I. S.; Van Tendeloo, G. Modified chitosan coated mesoporous strontium hydroxyapatite nanorods as drug carriers. *J. Mater. Chem. B* **2015**, *3*, 5991−6000.
(27) Zhang, C.; Li, C.; Huang, S.; Hou, Z.; Cheng, Z.; Yang, P.; Peng, C.; Lin, J. Self-activated luminescent and mesoporous strontium hydroxyapatite nanorods for drug delivery. *Biomaterials* **2010**, *31*, 3374−3383.
(28) Chen, C. C.; Liu, Y. C.; Wu, C. H.; Yeh, C. C.; Su, M. T.; Wu, Y. C. Preparation of fluorescent silica nanotubes and their application in gene delivery. *Adv. Mater.* **2005**, *17*, 404−407.
(29) Yang, X.; Tang, H.; Cao, K.; Song, H.; Sheng, W.; Wu, Q. Templated-assisted one-dimensional silica nanotubes: synthesis and applications. *J. Mater. Chem.* **2011**, *21*, 6122−6135.
(30) Hao, J.; Fang, X.; Zhou, Y.; Wang, J.; Guo, F.; Li, F.; Peng, X. Development and optimization of solid lipid nanoparticle formulation for ophthalmic delivery of chloramphenicol using a box-behnken design. *Int. J. Nanomedicine* **2011**, *6*, 683−692.
(31) Patil, S. S.; Dhumal, R. S.; Varghese, M. V.; Paradkar, A. R.; Khanna, P. K. Synthesis and antibacterial studies of chloramphenicol loaded nano-silver against *Salmonella typhi*. *Synth. React. Inorg., Met.-Org., Nano-Met. Chem.* **2009**, *39*, 65−72.
(32) Kadhim, Q. A.; Alwan, R. M.; Ali, R. A.; Jassim, A. N. Synthesis of zinc oxide/polystyrene nanocoposite films and study of antibacterial activity against *Escherichia coli* and *Staphylococcus aures*. *Nanosci. Nanotechnol.* **2016**, *6*, 1−5.
(33) Kolmas, J.; Groszyk, E.; Kwiatkowska-ró, D. Substituted Hydroxyapatites with Antibacterial Properties. *BioMed Res. Int.* **2014**, *2014*, No. 178123.
(34) Shinohara, T.; Shirahase, T.; Murakami, D.; Hoshino, T.; Kikuchi, M.; Koike, J.; Horigome, M.; Masunaga, H.; Ogawa, H.; Takahara, A. Characterization of surface microstructures on bio-based polymer film fabricated with nano-imprint lithography by synchrotron radiation small angle x-ray scattering. *IOP Conf. Ser.: Mater. Sci. Eng.* **2011**, *24*, No. 012004.
(35) Keller, S. S.; Feidenhans, L. N.; Fisker-Bødker, N.; Soulat, D.; Greve, A.; Plackett, D. V.; Boisen, A. Fabrication of biopolymer cantilevers using nanoimprint lithography. *Microelectron. Eng.* **2011**, *88*, 2294−2296.

DOI: 10.1021/acsomega.7b01756
ACS Omega 2018, 3, 1509−1521

(36) Yoshii, Y.; Waki, A.; Yoshida, K.; Kakezuka, A.; Kobayashi, M.; Namiki, H.; Kuroda, Y.; Kiyono, Y.; Yoshii, H.; Furukawa, T.; Asai, T.; Okazawa, H.; Gelovani, J. G.; Fujibayashi, Y. The use of nano-imprinted scaffolds as 3D culture models to facilitate spontaneous tumor cell migration and well-regulated spheroid formation. *Biomaterials* **2011**, *32*, 6052−6058.
(37) Ivanova, E. P.; Hasan, J.; Webb, H. K.; Gervinskas, G.; Juodkazis, S.; Truong, V. K.; Wu, A. H. F.; Lamb, R. N.; Baulin, V. A.; Watson, G. S.; Watson, J. A.; Mainwaring, D. E.; Crawford, R. J. Bactericidal activity of black silicon. *Nat. Commun.* **2013**, *4*, No. 2838.
(38) Hizal, F.; Zhuk, I.; Sukhishvili, S.; Busscher, H. J.; van der Mei, H. C.; Choi, C. Impact of 3D hierarchical nanostructures on the antibacterial efficacy of a bacteria-triggered self-defensive antibiotic coating impact of 3D hierarchical nanostructures on the antibacterial efficacy of a bacteria-triggered self-defensive antibiotic coating. *ACS Appl. Mater. Interfaces* **2015**, *7*, 20304−20313.
(39) Chopra, I.; Roberts, M. Tetracycline Antibiotics: Mode of Action, Applications, Molecular biology, and epidemiology of bacterial resistance tetracycline antibiotics: mode of action, applications, molecular biology, and epidemiology of bacterial resistance. *Microbiol. Mol. Biol. Rev.* **2001**, *65*, 232−260.
(40) May, P. W.; Clegg, M.; Silva, T. A.; Zanin, H.; Fatibello-Filho, O.; Celorrio, V.; Fermin, D. L.; Welch, C. C.; Hazell, G.; Fisher, L.; Nobbs, A.; Su, B. Diamond-coated 'black silicon' as a promising material for high- surface-area electrochemical electrodes and antibacterial surfaces. *J. Mater. Chem. B* **2016**, *4*, 5737−5746.
(41) Hayes, M. J.; Levine, T. P.; Wilson, R. H. Identification of nanopillars on the cuticle of the aquatic larvae of the drone fly. *J. Insect Sci.* **2016**, *16*, No. 36.
(42) Hasan, J.; Raj, S.; Yadav, L.; Chatterjee, K. RSC Advances superhydrophobic and superkilling properties. *RSC Adv.* **2015**, *5*, 44953−44959.
(43) Di Ciccio, P.; Vergara, A.; Festino, A. R.; Paludi, D.; Zanardi, E.; Ghidini, S.; Ianieri, A. Biofilm formation by *Staphylococcus aureus* on food contact surfaces: relationship with temperature and cell. *Food Control* **2015**, *50*, 930−936.
(44) Varna, D.; Psomas, G.; Choli-Papadopoulou, T.; Papi, R.; Hatzidimitriou, A. G.; Aslanidis, P. Dinuclear copper(I) complexes of N-methylbenzothiazole-2-thione: Synthesis, structures, antibacterial activity and DNA interactions. *J. Coord. Chem.* **2016**, *69*, 2500−2513.

DOI: 10.1021/acsomega.7b01756
ACS Omega 2018, 3, 1509−1521